Volume 14
Number 1
6 January 2026
Pages 1-296

Biomaterials Science

rsc.li/biomaterials-science

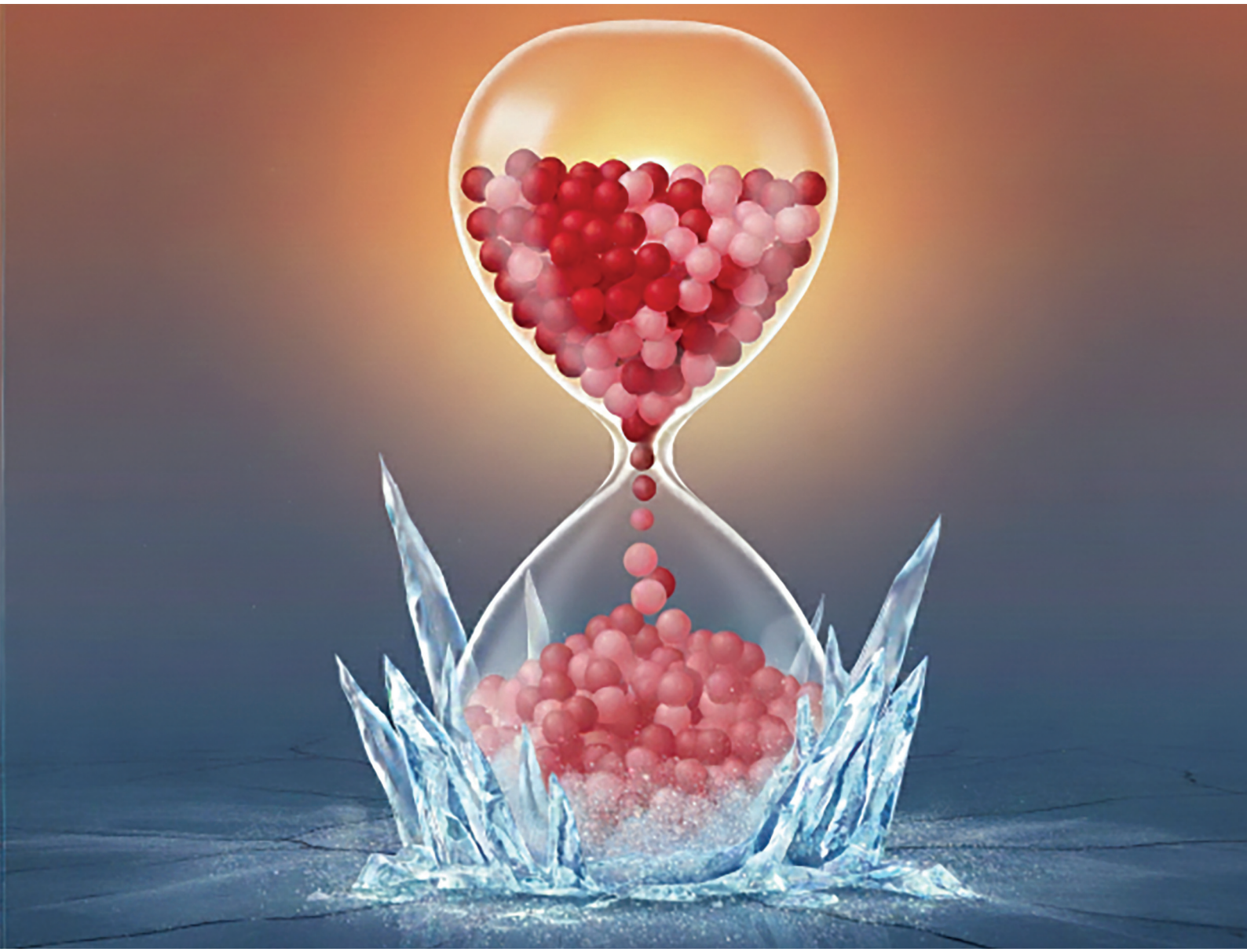

ISSN 2047-4849

ROYAL SOCIETY OF CHEMISTRY

PAPER

Annalisa Radeghieri *et al.*
Red blood cell-derived extracellular vesicles as biomaterials: the opportunity of freezing-induced accelerated aging

ESB European Society for Biomaterials

Biomaterials Science

ROYAL SOCIETY OF CHEMISTRY

PAPER

View Article Online
View Journal | View Issue

Cite this: *Biomater. Sci.*, 2026, **14**, 122

Red blood cell-derived extracellular vesicles as biomaterials: the opportunity of freezing-induced accelerated aging

Lucia Paolini, †[a,b] Miriam Romano,†[b,c,d] Valentina Mangolini,[d,e] Selene Tassoni,[d,b] Shuhan Jiang,[f,g] Elena Laura Mazzoldi, [d,h] Angelo Musicò,[d,b,i] Andrea Zendrini,[b,d] Anna Kashkanova,[f,g] Vahid Sandoghdar,[f,g,j] Anna C. Berardi,[k] Silvia Clara Giliani,[d,h,l,m] Paolo Bergese [d,b,m] and Annalisa Radeghieri *[d,b]

Red blood cell-derived extracellular vesicles (RBC-EVs) are emerging as promising biomaterials for next-generation drug delivery, owing to their intrinsic biocompatibility, immune-evasion properties, and minimal oncogenic risk. However, their broader application is currently limited by unresolved challenges related to heterogeneity, reproducibility, and long-term storage stability. By combining discontinuous sucrose density gradient separation with high-resolution interferometric nanoparticle tracking analysis, we identified a sharp bimodal size distribution of vesicles in freshly prepared samples. We then tracked how long-term storage at −80 °C drove their conversion into a monomodal distribution. To reproduce these conditions in a shorter time frame, we developed an "accelerated-ageing" protocol based on freeze–thaw cycles that generates RBC-EV samples with homogeneous density, size distribution, and biological activity, effectively replicating the properties of preparations stored for six months at −80 °C. This new vesicle population remains stable and retains membrane integrity and cellular internalization capacity, as confirmed by surface-associated enzymatic activity assays and uptake tests in cancer cell lines. These results suggest that freezing-induced "accelerated ageing" represents an effective method for the optimization and standardization of RBC-EVs as building blocks for biomaterial and bioengineering applications.

Received 5th September 2025,
Accepted 20th November 2025

DOI: 10.1039/d5bm01349f

rsc.li/biomaterials-science

[a]*Dept. of Medical and Surgical Specialties, Radiological Sciences and Public Health (DSMC), University of Brescia, Brescia, Italy*
[b]*Center for Colloid and Surface Science, (CSGI), Sesto Fiorentino (FI), Italy. E-mail: annalisa.radeghieri@unibs.it*
[c]*ASST Spedali Civili di Brescia, Dept. of Emergency, Spedali Civili University Hospital, Brescia, Italy*
[d]*Dept. of Molecular and Translational Medicine (DMMT), University of Brescia, Brescia, Italy. E-mail: annalisa.radeghieri@unibs.it*
[e]*IRCCS Fondazione Don Carlo Gnocchi ONLUS, Milano, Italy*
[f]*Max-Planck-Institut für die Physik des Lichts, 91058 Erlangen, Germany*
[g]*Max-Planck-Zentrum für Physik und Medizin, 91058 Erlangen, Germany*
[h]*"Angelo Nocivelli" Institute for Molecular Medicine, ASST Spedali Civili, 25123 Brescia, Italy*
[i]*Istituto di Scienze e Tecnologie Chimiche "Giulio Natta" – National Research Council of Italy (SCITEC-CNR), Milan, Italy*
[j]*Department Physik, Friedrich-Alexander Universität Erlangen, Nürnberg, 91058 Erlangen, Germany*
[k]*Laboratory of Stem Cells, U.O.C. of Immunohaematology and Transfusion Medicine, Santo Spirito Hospital, Pescara, Italy*
[l]*Section of Medical Genetics and Cytogenetics, ASST Spedali Civili of Brescia, 25123 Brescia, Italy*
[m]*National Center for Gene Therapy and Drugs based on RNA Technology, Padua, Italy*
†These authors equally contributed to the work.

1. Introduction

Extracellular vesicles (EVs) are a groundbreaking biological discovery of the past two decades. These natural lipid nanoparticles, ranging in size from 30 nm to 1000 nm, are secreted by all cell types in animals and bacteria, acting as carriers for many biomolecules.[1] EVs play a vital role in mediating physiological processes and contributing to disease spread, including cancer[2] and infections.[3] Their unique properties, which have evolved for efficient transport and pharmacokinetics, make them highly promising for precision nanomedicine.[4] Early clinical trials of EV-based therapeutics have shown encouraging results, fueling ongoing research into their potential as novel biomaterials, *i.e.*, as drug delivery vehicles.[5,6]

Red blood cell-derived EVs (RBC-EVs) stand out as particularly promising biomaterials for next-generation drug delivery,[6] offering several key advantages: they are devoid of mitochondrial and nuclear DNA, thus posing minimal oncogenic risk, and exhibit excellent biocompatibility.[7–10] RBC-EVs can be produced at a large scale with good reproducibility and benefit from well-established protocols in transfusion medicine.[11]

Additionally, RBC-EVs derived from patients' blood offer precision and safety, making them an attractive option for clinical translation in drug delivery and therapeutic applications.

Large-scale *in vitro* production of RBC-EVs can be boosted by exploiting external stimuli (*i.e.*, physical or chemical stress).[12] The main chemical inducers used so far in this context are calcium ionophores, such as ionomycin and A23187,[13] lysophosphatidic acid (LPA),[14] and phorbol-12 myristate-13 acetate (PMA).[15] This procedure is then followed by the separation of RBC-EVs from RBCs by different methods, which usually include serial ultra-centrifugation steps and a sucrose gradient.[8]

Compared to naturally secreted RBC-EVs obtained after RBC storage[16,17] for up to 28 days at +4 °C, chemically induced RBC-EVs show a very similar enrichment of EV markers, with sizes and shapes typical of EVs.[8,18] Furthermore, the biochemical composition obtained by proteomic analysis looks very similar, apart from the enrichment of calcium-binding proteins[19] and some differences in membrane protein expression.[20]

Despite earlier findings,[18] it has recently been shown that fresh chemically induced RBC-EVs exhibit two separate size and density profiles, each with distinct protein expression patterns. These variations lead to differing physiological responses upon internalization.[21] In addition, it has been demonstrated that different storage conditions can impact EV yield, physical properties, and functionality,[22] and combined technologies are needed to characterize all the modifications occurring in EV samples.[23]

Thus, in order to enable biobanking of RBC-EVs for large-scale production and use, it is essential to conduct extensive studies on their homogeneity and stability under different storage conditions. These factors are crucial, as different storage protocols can significantly influence the biological activity of RBC-EVs.[24–26] Additionally, to ensure the therapeutic applicability of RBC-EVs in large quantities, it is necessary to evaluate whether their heterogeneity persists during storage and whether maintaining this heterogeneity is beneficial. For clinical use, however, a more homogeneous product may be preferable to ensure consistent therapeutic outcomes[27] according to international medicines regulatory agencies' guidelines.[28,29]

In order to achieve this, key technologies for single-vesicle or subpopulation-level analysis have been developed, such as high-sensitivity flow cytometry[30] and NanoFlow cytometry (NanoFCM),[31] which enable size and surface-marker profiling. ExoView,[32] a chip-based immunocapture platform, allows multiplexed phenotyping of individual EVs without extensive preprocessing. Structural heterogeneity can be explored *via* atomic force microscopy (AFM)[33] and electron microscopy (EM),[34] which provide nanoscale resolution. Raman and FT-IR spectroscopy[35,36] offer label-free biochemical fingerprints, while surface plasmon resonance (SPR)[37] detects molecular interactions in heterogeneous EV populations.

Recently, interferometric nanoparticle tracking analysis (iNTA) has been introduced in this scenario with the advantage of high-precision measurement of EV size and content by refractive index determination.[38,39] Employing at least two orthogonal analytical methods is widely recommended to minimize methodological bias.

In this study, by combining multiparametric characterization based on iNTA and a discontinuous density gradient (DSG), we developed an "accelerated-ageing" protocol based on freeze–thaw cycles that allows the generation of highly homogeneous RBC-EV preparations. These preparations were assessed for RBC-EV membrane preservation using a RBC-EV surface-associated enzymatic assay and for their capacity to be internalized by cells.

2. Materials and methods

We have submitted all relevant data from our experiments to the EV-TRACK knowledge base (EV-TRACK ID: EV250035).[40]

2.1 RBC-EV production

RBC-EVs were isolated according to the protocols outlined by previous works.[8,18] In brief, after the collection of 100 ml of blood, red blood cells (RBCs) were separated by centrifugation at 1000*g* for 8 min at 4 °C and washed three times in PBS without calcium and magnesium. Following this, RBCs were subjected to two additional washes with CPBS (PBS + 0.1 g L^{-1} calcium chloride) and then transferred into a 75 mm^2 tissue culture flask. Calcium ionophore was added to the flask at a final concentration of 10 μM, and the mixture was incubated overnight at 37 °C. Subsequently, 75 ml of RBCs were gently collected from the flask, and any cellular debris was eliminated through a series of differential centrifugation steps (600*g* for 20 min, 1600*g* for 15 min, 3260*g* for 15 min, and 10 000*g* for 30 min at 4 °C). At each step, the pellet was discarded, and the supernatant was transferred into a fresh tube. The resulting supernatants were filtered through a sterile 0.45 μm nylon syringe filter. EVs were obtained through ultracentrifugation at 50 000*g* for 70 min at 4 °C. The EV pellets were then resuspended in cold PBS, layered above a 2 ml frozen 60% sucrose cushion, and centrifuged at 50 000*g* for 16 h at 4 °C, with the deceleration speed set to 0. The red layer of EVs was collected, washed twice with cold PBS, and spun down at 50 000*g* for 70 min at 4 °C. Finally, the EVs were resuspended in 1 ml of cold PBS and stored at 4 °C (fresh samples), at −80 °C for 6 months (6-month samples), or at −80 °C for 1 year (1-year samples) for further analyses. Red blood cells were obtained from five anonymized healthy volunteers (3 males, 3 females; age ranging from 36 to 59 years; mean age 50.8 years). All experiments were performed in accordance with the Declaration of Helsinki and were approved by the ethics committee at the A.O. Spedali Civili di Brescia, ID "EritrEV NP5705". Informed consent was obtained from the human participants in this study.

2.2 Freeze–thaw cycles

Fresh RBC-EV preparations, stored at 4 °C (maximum time 1 week), were subjected to two types of freeze-and-thaw cycles:

Light_5 cycles at −80 °C and 37 °C (water bath), 5 min each incubation; Strong_10 cycles at −80 °C and 37 °C (water bath), 5 min each incubation, before further analyses.

2.3 Bicinchoninic acid (BCA) and Bradford assay

Protein concentrations of the samples were determined using a Pierce™ BCA Protein Assay Kit (ThermoFisher, Rockford, USA) and a Bradford assay kit (Biorad) following the manufacturers' instructions.

2.4 Discontinuous density gradient (DSG)

DSG was carried out by adapting the protocols developed in the previous studies.[41,42] RBC-EVs produced as previously described were quantified using the Bradford assay, and then 600 μg were centrifuged at 50 000*g* at 4 °C for 70 min. Briefly, RBC-EV preparations were resuspended in buffer A (10 mM Tris-HCl, 250 mM sucrose, pH 7.4) to a final volume of 1 ml and loaded on top of a discontinuous sucrose density gradient (15% (600 μl), 20%, 25%, 30%, 40%, 60%, 65% (400 μl), and 70% (800 μl) sucrose in 10 mM Tris-HCl, pH 7.4). The gradient was centrifuged at 230 000*g* for 16 h at 4 °C (rotor MLS 50; Beckman Optima MAX-XP, no brake). Twelve fractions of equal volumes (400 μl) were collected from the top of the gradient. All fractions were diluted with 600 μl water to make them suitable for high-performance liquid chromatography (HPLC-grade water, final volume 1 ml) and ultracentrifuged at 100 000*g* for 2 h at 4 °C (Optima MAX-XP, TLA-55 rotor, 1.5 ml polypropylene microfuge tube, Beckman). Pellets were resuspended in 100 μl of HPLC-grade water previously ultracentrifuged at 100 000*g* for 2 h in an Optima MAX, TLA-55 rotor, 1.5 ml polypropylene microfuge tubes (Beckman), and aliquoted for further analyses.

2.5 SDS-PAGE and western blot analysis

SDS-PAGE and western blot analyses were performed according to standard procedures.[43,44] Both RBC-EV homogenates (H) and RBC-EV gradient fractions were denatured with 6× Laemmli buffer and boiled for 5 min at 95°. A total of 30 μg of RBC-EV homogenate was loaded, while 15 μl was loaded for each gradient fraction. Samples were electrophoresed on 12.5% acrylamide-bisacrylamide gels and analyzed by western blotting with the following antibodies (at 1 : 500 dilution): mouse anti-Flotillin 1 (Santa Cruz Biotechnology, clone C-2, sc-74566), rabbit anti-ADAM10 (Origene, AP05830PU-N), mouse anti-CD81 (Santa Cruz Biotechnology, clone B11, sc-166029), mouse anti-CD9 (Santa Cruz Biotechnology, clone C-4, sc-13118), mouse anti-TSG101 (Santa Cruz Biotechnology, clone C-2, sc-7964), mouse anti-LAMP1 (BD Biosciences, 611042/611043), mouse anti-Annexin V (Santa Cruz Biotechnology, clone H-3, sc-74438), rabbit anti-Annexin XI (Genetex, CTX33010), mouse anti-Alix (Santa Cruz Biotechnology, clone 2H12, sc-53539), mouse anti-CD45 (Santa Cruz Biotechnology, clone 35-Z6, sc-1178), mouse anti-Integrin αIIb/ITGA2B/CD41 (Santa Cruz Biotechnology, clone B-9), mouse anti-GAPDH (Millipore, clone 6C5), and mouse anti-Band 3 (Santa Cruz Biotechnology, clone A-6, sc-133190). Mouse anti-hemoglobin A (Abnova, clone 4F9) and mouse anti-hemoglobin B (Abnova, clone 7B12) were diluted to 1 : 1000. The blots were detected using a Luminata Classic HRP western substrate (Millipore). The images were acquired using a G:Box Chemi XT imaging system, as previously described.[45,46]

2.6 UV-VIS spectroscopy

RBC-EV gradient fractions were collected and treated as described above. Resuspended pellets were analyzed for the presence of hemoglobin by measuring the absorbance at 414 nm with a UV-VIS spectroscopy Nanodrop spectrophotometer (Thermo Scientific) as previously described.[47]

2.7 Colorimetric nanoplasmonic (CONAN) assay

The purity of RBC-EV preparations from soluble contaminants was tested with the CONAN assay according to Zendrini *et al.*[48,49] The assay is a colorimetric test that exploits the aggregation of citrate-capped gold nanoparticles (AuNPs) onto the EV membrane and the formation of a protein corona on the AuNP surface to detect soluble proteins in EV preparations.[49] Results of the assay were collected on an Ensight MultiMode Reader (PerkinElmer). Measurements were performed for each sample in triplicate and expressed as the mean of three replicates ± standard deviation.

2.8 Atomic force microscopy (AFM)

Atomic force microscopy (AFM) imaging was performed with a Nanosurf NaioAFM equipped with a Multi75-AI-G tip (Budget Sensors). For sample preparation, RBC-EV (bulk) pellets were resuspended in 100 μL of sterile H_2O (Milli-Q, Merck Millipore) and diluted 1 : 10 in H_2O. 5 μL of the sample were then spotted onto freshly cleaved mica sheets (Grade V-1, thickness 0.15 mm, size 15 × 15 mm^2) and air-dried at 37 °C for 10 min. Images were acquired in tapping mode, with a scan size ranging from 1.5 to 25 mm and a scan speed of 1 s per scanning line.[36] Image processing was performed on Gwyddion ver. 2.61.

2.9 Nanotracking particle analysis (NTA)

RBC-EV preparations were resuspended in 100 μl of sterile HPLC-grade water (Milli-Q; Merck Millipore) for characterization by Nanoparticle Tracking Analysis (NTA) using a NanoSight NS300 system (Malvern, Panalytical Ltd, Malvern, UK) to evaluate the concentration and size distribution of EVs. The system was equipped with a Blue488 laser and an sCMOS camera. Before sample analysis, filtered PBS (filtered with pore size 0.2 μm) was analysed for particle contamination. For the analysis, all samples were diluted in filtered PBS (1 : 1000) to a final volume of 1 ml to obtain the optimal particle number per frame value (20–120 particles per frame). EVs were injected into the sample chamber through a Nanosight syringe pump (Malvern Panalytical Ltd, Malvern, UK) that provides a continuous flow (50 μl min^{-1}) using a 1 ml syringe at room temperature. Recordings of the movements of particles were performed for 60 s, five times for each sample, at a camera level of 12 using the best detection threshold. The mean, mode, and

median EV sizes from each video were used to calculate the sample concentration, expressed in particles per ml.[50]

2.10 Interferometric nanoparticle tracking analysis (iNTA)

Samples (at least 3 biological replicates for each point analyzed) were diluted to 1 : 100 and analyzed using the iNTA instrument.[38] An iNTA measurement setup was utilized for particle analysis.[51] Measurements were conducted using IBIDI μ-Slide 18-well chambered cover glasses, which were plasma-cleaned and passivated with an mPEG2000-Silane (Laysan Bio) solution.[39] The microscope focus was adjusted to 1 μm above the cover glass, and 100 μL of diluted RBC-EVs were observed over 30 min. Measurements were performed at 10 kHz with a 50 μs exposure time. The field of view (FOV) was 6 × 6 μm^2. Particle size was derived from the diffusion constant. Contrast$^{1/3}$ was calculated as the ratio of the scattered field to the reflected field.

2.11 MDA-MB-231 cell culture

The MDA-MB-231 cell line was purchased from the American Type Culture Collection (ATCC; Manassas, VA, USA). For culture maintenance, cells were cultured in Dulbecco's Modified Eagle Medium (DMEM) with 4.5 g L^{-1} glucose, L-glutamine and sodium pyruvate (Corning, USA), supplemented with 1% penicillin–streptomycin and 10% fetal bovine serum (FBS, EuroClone S.p.A., Italy).

2.12 RBC-EV labelling

RBC-EV labeling with MemGlow™ 488 was performed following the standard customer protocols as previously described.[8] Briefly, fresh, 6-month, and Strong F–T RBC-EV samples (10^{11} particles per sample) were incubated with 5 μl of MemGlow™ 488, 100 nM, for 15 min at RT (final volume 1 ml in PBS), and then excess MemGlow™ 488 was removed by ultracentrifugation (100 000*g*, 2 h, Optima MAX-XP equipped with a TLA-55 rotor, Beckman Coulter, USA). Before cell treatments, pellets were resuspended in 500 μl DMEM serum-free medium.

2.13 Flow cytometry

MDA-MB-231 cells were seeded in a 12-well plate, 4 × 10^5 cells per well, in 1 ml of complete medium. After 24 h, MDA-MB-231 cells were washed twice with PBS and incubated for either 30 min or 4 h with MemGlow™ 488-stained fresh/6-month/strong F–T RBC-EVs (10^{11} RBC-EVs per well; 500 μl final volume), unstained fresh RBC-EVs (10^{11} RBC-EV), or MemGlow™ 488 fluorescent dye without RBC-EVs. The treatment with MemGlow™ 488 fluorescent dye without EVs was performed to exclude any possible nonspecific fluorescent signals. Untreated cells were used as a negative control. After incubation, cells were washed with PBS and treated with 200 μl of 0.25% trypsin–EDTA (Corning, USA) for 1 min at 37 °C to remove externally bound EVs and to detach the cells from the culture vessel. After trypsin treatment, cells were resuspended in 500 μl of DMEM medium supplemented with 5% fetal bovine serum and centrifuged at 800*g* for 5 min. Pellets were resuspended in 200 μl of serum-free DMEM and analyzed by flow cytometry. Flow cytometry acquisition was performed on FACSCanto™ II (BD, Franklin Lakes, NJ) from at least 2 × 10^4 events/tube, excluding debris, dead cells and doublets. Data were processed using FlowJo v10.6.2 software (TreeStar, Ashland, OR). The results were expressed as the difference between the median fluorescence intensity of cells incubated with MemGlow™ 488-stained RBC-EVs and that of the corresponding untreated control (ΔMFI).

2.14 Acetylcholinesterase activity assay

Acetylcholinesterase activity was assessed by standard procedures.[52,53] Briefly, 3 × 10^9 particles of fresh RBC-EVs, 6-month RBC-EVs stored at −80 °C and after Strong F–T treatment, were diluted in 60 μl of PBS without calcium and magnesium and incubated with 1.25 mM acetylthiocholine (Sigma-Aldrich) and 0.1 mM 5,5′-dithio-bis(2-nitrobenzoic acid) in a final volume of 1 ml. The incubation was carried out in 96-well plates at 37 °C, and the change in absorbance at 415 nm was monitored at 0, 10, 20, 30, and 60 min. Absorbance was measured with a Model 680 spectrophotometer (Bio-Rad, USA). Data are presented as the mean of three technical replicates ± standard deviation (SD).

2.15 Statistical analysis

For the iNTA and flow cytometry analyses, statistical analysis was performed using Student's *t*-test: $^{**}p$ value ≤ 0.01, $^{***}p$ value ≤ 0.001, $^{****}p$ value < 0.0001, ns = not significant. For the measurements of the mean diameters of the RBC-EV fractions calculated with NTA, the statistical analysis was performed with ordinary one-way ANOVA. $^{****}p$ value < 0.0001. All statistical analyses were performed using GraphPad Prism software.

3. Results and discussion

3.1 Fresh RBC-EV production and characterization

Red blood cell-derived EVs (mean concentration: 9 × 10^{11} ± 3 × 10^9 RBC-EVs per ml, measured by NTA) were obtained following the protocol described by Usman *et al.*[18] from the RBCs of five healthy volunteers (three males and three females, aged from 36 to 59 years, with a mean age of 50.8 years) and stored at +4 °C for a maximum of 1 week (fresh). Preparations were characterized according to the most updated guidelines.[54] In particular, western blot analysis was used to identify the presence or absence of specific protein markers. Specifically, RBC-EVs were found to express Band 3, GAPDH, hemoglobin subunit β (HBB), hemoglobin subunit α (HBA), Flotillin-1, Annexin V, LAMP-1, Annexin XI, and ADAM10. Among these, Band 3, HBB, and HBA are specific markers of RBC-EVs, while the others represent common markers of EVs.[1,11,54] In contrast, the RBC-EV preparations did not express CD45, a typical marker of leukocytes, nor CD41, a platelet-specific marker, indicating that the RBC-EV preparations were free from contamination by other blood components.[55] Additionally, the RBC-EVs lacked the tetraspanins CD9 and CD81, which aligns with findings in the existing literature[56] (Fig. 1A). The

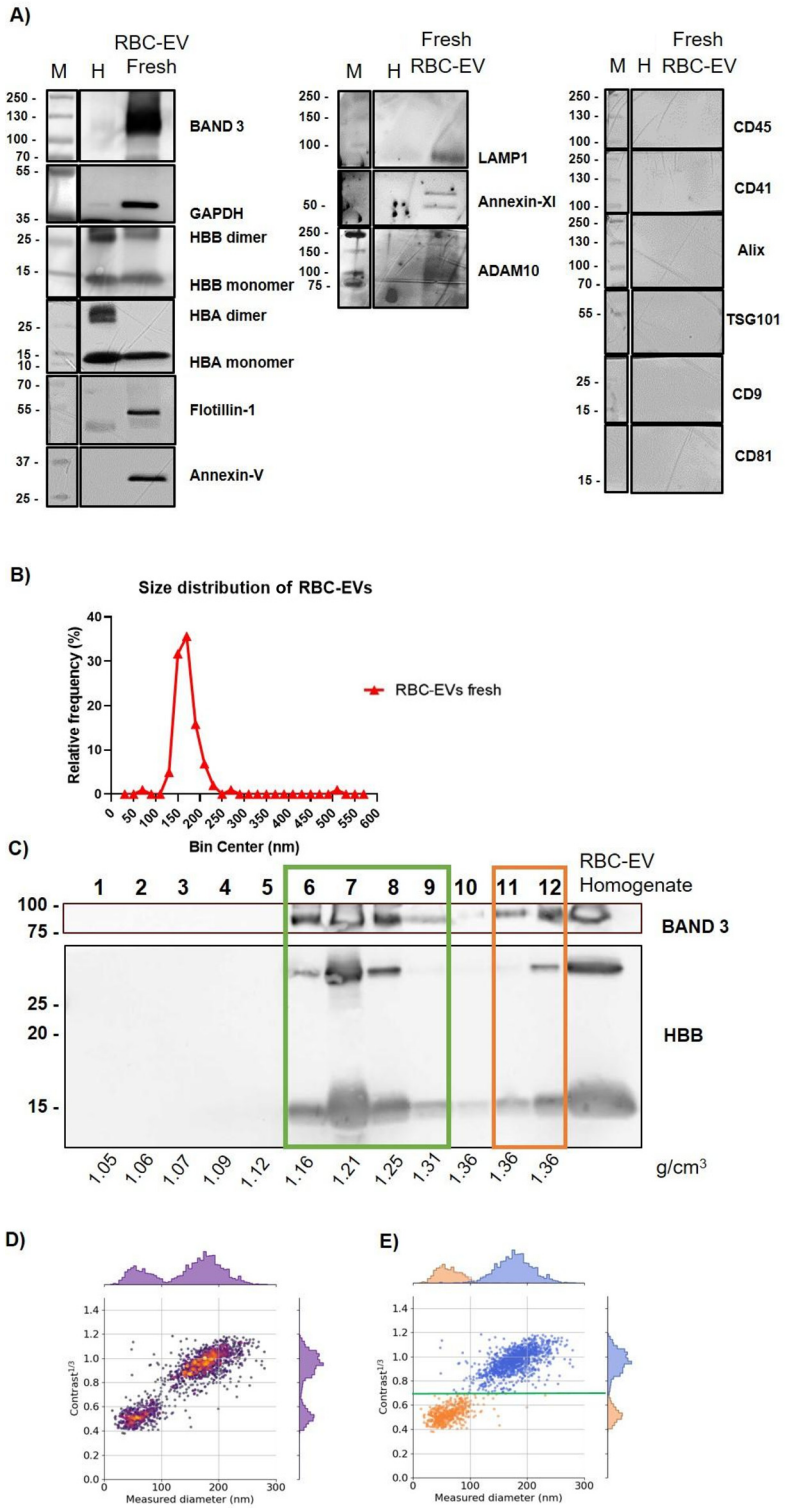

Fig. 1 Fresh RBC-EV characterization. (A) Biochemical characterization of RBC-EVs stored at 4 °C for 1 week (fresh) preparations; M = marker; H = cellular homogenate (30 μg). (B) Size distributions of fresh RBC-EVs. Size distributions obtained by Nanoparticle Tracking Analysis (NTA). (C) Identification of two subpopulations by western blot of Discontinuous Sucrose Gradient (DSG) fractions of fresh RBC-EV preparations. Proteins detected are Band 3 anion transport protein (BAND3) and hemoglobin subunit β; RBC-EV homogenate loaded (30 μg). Green box: RBC-EV fractions with a density from 1.16 to 1.31 g cm^{-3}; orange box: RBC-EV fractions with a density of 1.36 g cm^{-3}. (D) Size distribution and contrast measurements of fresh RBC-EVs obtained with iNTA. (E) Identification of two fresh RBC-EV subpopulations with different sizes and contrast by iNTA. Orange dots: EVs with a size from 30 to 100 nm and contrast below 0.7; blue dots: EVs with a size from 101 to 300 nm and contrast from 0.71 to 1.4.

Bradford assay and the Colorimetric Nanoplasmonic (CONAN) assay[48,49] (Fig. S1A and B) were used to determine protein concentration and the absence of soluble protein contaminants, respectively, while Atomic Force Microscopy (AFM) was implemented to investigate the morphology of the nano-objects in the preparations (SI Fig. S1C). The data were in accordance with our previous works.[8,57] In addition, the samples were analyzed for their nanoparticle size distribution using Nanoparticle Tracking Analysis (NTA). The results shown in Fig. 1B highlighted that, with this analytical technique, we cannot detect significant differences in terms of subpopulation heterogeneity since all samples showed a median homogeneous distribution around 165 ± 13.2 nm. These data were in contrast with previous findings about freshly isolated RBC-EVs stored at +4 °C,[21] indicating that, probably, conventional NTA alone may not be the best option to investigate subpopulation heterogeneity. Therefore, different methods with higher sensitivity and better resolution are needed.[38,58]

3.2 Orthogonal methods reveal heterogeneity in freshly isolated RBC-EVs

In order to investigate the heterogeneity of RBC-EV preparations, two different bio-orthogonal techniques were introduced: discontinuous sucrose density gradient (DSG), which allows differentiation of RBC-EVs on their density[41,42] and interferometric NTA (iNTA). According to the recent literature, different RBC-EV populations can be identified using optical methods.[21] We, thus, decided to perform iNTA analysis on the RBC-EV preparations. This method allowed us to differentiate nanoparticles by their size and interferometric contrast (contrast$^{1/3}$). In addition, this method has been demonstrated to exhibit higher sensitivity and better resolution for determining the size distribution of small nanoparticles compared to conventional NTA.[38,39]

Fresh RBC-EV preparations were loaded on top of a DSG separately and centrifuged for 16 h at 230 000*g*. Twelve fractions of equal volume (400 µl) were collected, processed as described in Materials and Methods, and analyzed for their biomolecular profile, density,[41,59] particle number and size distribution. As shown in Fig. 1C, western blot analysis for typical RBC-EV markers Band 3 and HBB[18,21,33] of the 12 fractions revealed the presence of two subpopulations: one distributed within fractions bearing densities from 1.16 to 1.31 g cm^{-3} (fractions 6–9, green box) and the other with a density around 1.36 g cm^{-3} (fractions 11 and 12, orange box). Band 3 and HBB signals, both in the monomeric form (detected at 15 kDa) and dimeric form (detected at 30 kDa), were perfectly matching across the fractions. The hemoglobin distribution of RBC-EVs in the DSG fractions was also analyzed by UV-VIS spectroscopy absorbance at 414 nm. Results confirmed the distribution highlighted in the western blot with a peak of absorption in fraction 7 (SI Fig. S2A). NTA analysis of DSG fractions confirmed an enrichment of nanoparticles in fractions 6–7 (SI Fig. S2B), and the BCA assay confirmed the presence of proteins, especially in fraction 7 (SI Fig. S2C).

Measurements on fresh samples obtained with iNTA aligned perfectly with the DSG distribution, even though the two methods assess different physical and chemical properties, since DSG focuses on density, while iNTA measures contrast and size distribution.

As shown in Fig. 1D and E, RBC-EVs showed a bi-modal distribution when contrast$^{1/3}$ is plotted *vs.* hydrodynamic size for each nanoparticle. We could demonstrate the presence of two subpopulations: one with contrast$^{1/3}$ below 0.7 and a size distribution mostly below 100 nm (Fig. 1E, orange dots, lower subpopulation) and another with contrast$^{1/3}$ above 0.7 and a size distribution mostly above 100 nm (Fig. 1E, blue dots, upper subpopulation).

3.3 Long-term storage conditions at −80 °C affect RBC-EV heterogeneity

With the objective of homogenizing RBC-EVs for use as a standardized biomaterial, we evaluated whether long-term storage at −80 °C could affect this parameter. We conserved RBC-EV preparations for 6 months at −80 °C (6-month samples) or 1 year at −80 °C (1-year samples).

We next evaluated subpopulation heterogeneity, applying the same orthogonal methods as for the fresh samples. First, compared to the fresh sample (Fig. 2A), the 6-month sample showed a different distribution among the DSG fractions in western blot: protein signals in fractions at higher density (11 and 12) were no longer present (Fig. 2B). Instead, both Band 3 and HBB remained distributed in fractions 6–8, with an additional presence in lighter fractions, particularly fractions 4 and 5 (density 1.09–1.12 g cm^{-3}). This shift was especially noticeable for the Band 3 signal (detected at 95 kDa) and the monomeric form of hemoglobin (detected at 15 kDa) (Fig. 2B, blue box). These results were confirmed through spectroscopic analysis of the hemoglobin content that showed a peak of absorption in fraction 5 (SI Fig. S2A). NTA measurements indicated an enrichment of nanoparticles in fractions 4 and 5 (SI Fig. S2B), at higher concentrations with respect to the fresh samples. Likewise, the BCA assay confirmed a higher protein concentration in fraction 5 relative to the fresh sample (SI Fig. S2C).

A similar trend was observed for the 1-year sample, which showed an even more pronounced narrowing of the RBC-EV distribution in the DSG fractions (from fractions 4 to 7; corresponding to a density of 1.09–1.21 g cm^{-3}) (Fig. 2C, black box) and a consequential disappearance of the Band 3 signal from fractions 8 and 9 and a reduction of the hemoglobin signal in these two fractions. Uncropped versions of the western blot images described so far can be found in SI Fig. S3A–C.

Spectroscopic analysis of the hemoglobin content aligned perfectly with these observations, confirming a decrease in the hemoglobin in these two fractions (SI Fig. S2A) and an increased signal in fractions 5 and 6 compared to the fresh sample. NTA and protein measurements confirmed the results with an increased concentration of nanoparticles in fractions 4 and 5 and in fractions 5 and 6, respectively, compared to the fresh sample (SI Fig. S2B and C).

In addition, NTA analysis of DSG fractions from 4 to 7 highlighted changes in size distribution between the three RBC-EV preparations. Indeed, DSG fractions of the fresh RBC-EV

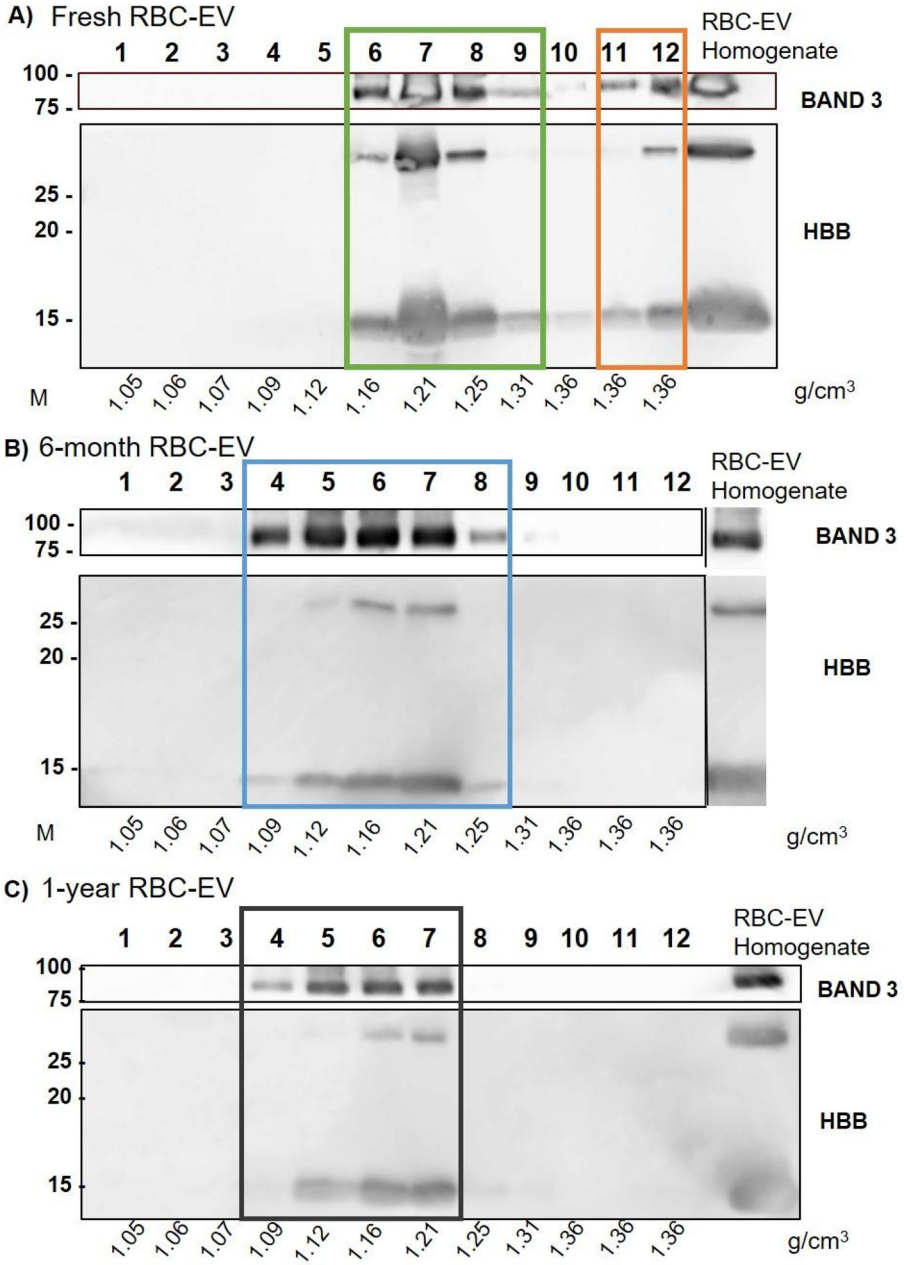

Fig. 2 Gradient distribution of RBC-EVs under different storage conditions. Western blot of RBC-EVs after DSG; equal volumes (15 μL) of each fraction (1–12) for (A) fresh, (B) 6-month, and (C) 1-year samples were loaded; 30 μg of RBC-EV homogenate samples were loaded. Samples were electrophoresed on 12% SDS-PAGE gel (acrylamide/bis-acrylamide) and analyzed with the antibodies described in the figures. Uncropped WBs are available in the SI (Fig. S3). Each fraction density is indicated in g cm^{-3}. Protein molecular weight marker (M) indicated on the left of the gel (kDa). RBC-EV subpopulations with different gradient distributions are indicated in colored boxes: (A) green box: fractions 6–9; orange box: fractions 11–12; (B) blue box: fractions 4–9; and (C) black box: 4–7.

samples showed the presence of two statistically significant subpopulations in fractions 4–5 compared to fractions 6–7 (SI Fig. S4A). Particles in fractions 4–5 exhibit a mean size of 123 ± 51 nm, while particles in fractions 6–7 exhibit a mean diameter of 170 ± 10 nm (SI Fig. S4B). On the other hand, the 6-month and 1-year samples did not exhibit the dual size distribution in fractions 4–5 and 6–7 observed in the fresh samples (SI Fig. S4C–F).

Taken together, these data indicate that the RBC-EV subpopulations undergo significant changes in their distribution and composition during long-term storage, with a shift toward lighter fractions, reduced density and modulated size of the particles, suggesting potential alterations in RBC-EV heterogeneity over time.

iNTA measurements further corroborated these data, showing that the separation into two distinct subpopulations

becomes significantly less prominent in samples that have been stored at −80 °C. Nevertheless, we can quantify the relative amount of nanoparticles with contrast$^{1/3}$ above and below 0.7 in all samples.

The fresh sample (Fig. 3A) showed that around 70% of the relative concentration of RBC-EVs was found in the upper population (Fig. 3G, contrast$^{1/3}$ > 0.7, blue dots), while 30% was distributed in the lower population (Fig. 3G, contrast$^{1/3}$ < 0.7, orange dots).

The 6-month sample showed an opposite distribution compared to the fresh sample (Fig. 3B and E): fewer nanoparticles were distributed in the upper population (Fig. 3G, contrast$^{1/3}$ >

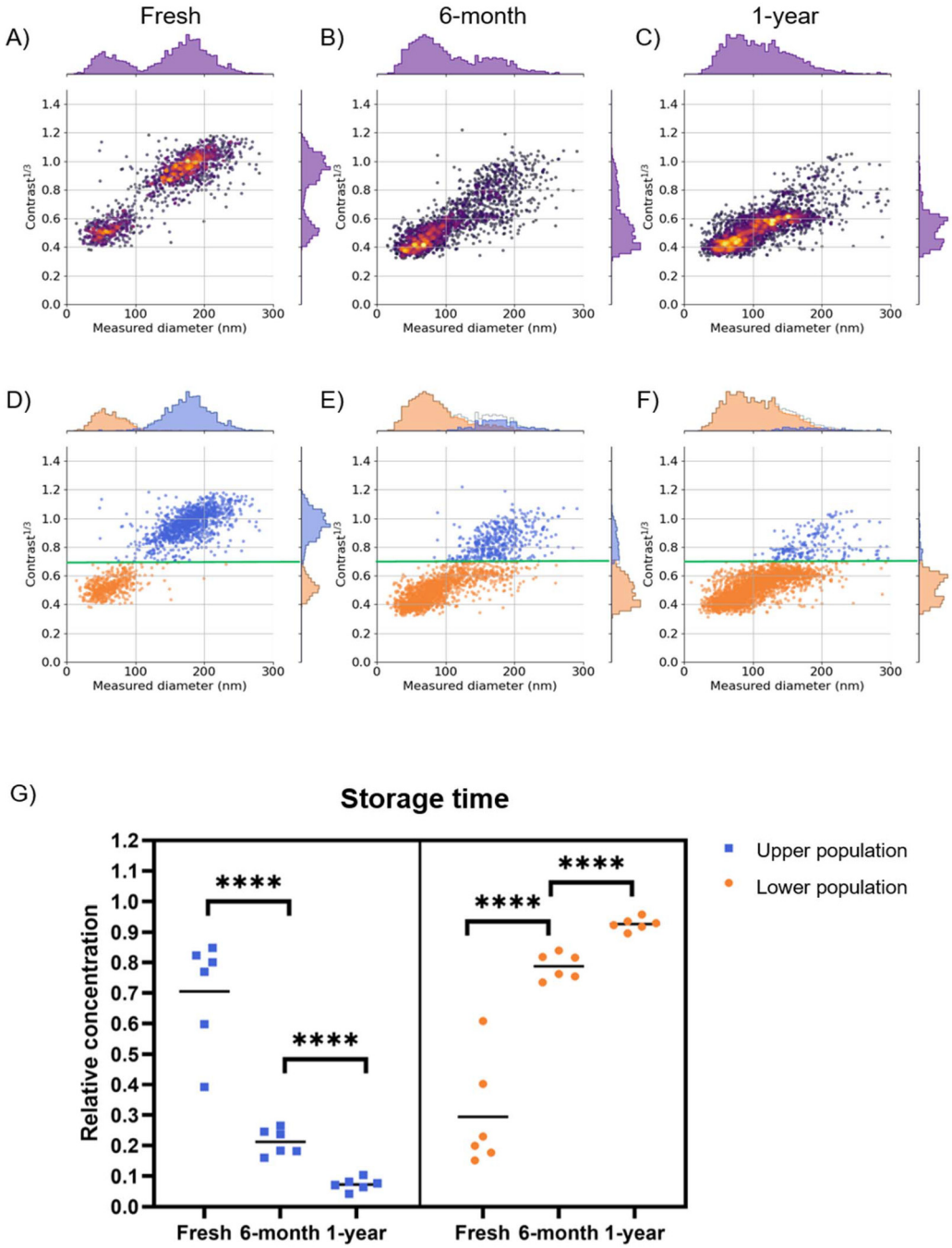

Fig. 3 Interferometric NTA (iNTA) analysis. Fresh (A), 6-month (B), and 1-year (C) samples were analyzed by iNTA. Images represent size distribution (*x*-axis) and contrast (*y*-axis) of the nanoparticles. Nanoparticle subpopulations grouped by contrast in fresh (D), 6-month (E), and 1-year (F) samples. The green line represents a contrast$^{1/3}$ value of 0.7. Nanoparticle distribution determined for contrast$^{1/3}$ >0.7 (blue dots, upper population) or <0.7 (orange dots, lower population). (G) Relative quantification of nanoparticles present in the upper (contrast$^{1/3}$ >0.7) and lower (contrast$^{1/3}$ <0.7) population for fresh, 6-month, and 1-year samples. Statistical analysis using Student's *t*-test: ****p value < 0.0001.

0.7, blue dots) compared to the fresh sample, with their relative concentration decreasing to 20% (Fig. 3G, blue dots). Meanwhile, the relative concentration of the lower population (contrast$^{1/3}$ < 0.7) increased to 80% of the total nanoparticles analyzed (Fig. 3G, $p < 0.0001$). This trend was even more pronounced in the 1-year sample: only 10% of nanoparticles were distributed in the upper population, while 90% were found in the lower population. The shift in distribution between the 6-month and 1-year samples was also statistically significant (Fig. 3G, $p < 0.0001$).

These data are in accordance with the DSG distribution and confirm that storage reduces the heterogeneity of RBC-EVs. Over time, the two distinct subpopulations gradually merge into a more uniform population in terms of density and contrast$^{1/3}$, with this shift becoming more pronounced in a time-dependent manner.

3.3 Freeze–thaw cycles decrease RBC-EV heterogeneity

To develop a method that ensures consistent conditions in RBC-EV preparations similar to those found in long-term stored samples, without the need for prolonged storage, we exposed fresh samples to two different types of freeze/thaw (F–T) cycles. The first treatment, labeled "Light F–T", involved 5 cycles at −80 °C and 37 °C, each lasting 5 min. The second treatment, labeled "Strong F–T", involved 10 cycles at the same temperatures and duration. The samples were then analyzed by DSG to biochemically confirm the changes in the density distributions and by iNTA to assess changes in the relative concentrations in terms of contrast$^{1/3}$ of the subpopulations of RBC-EVs. Notably, the Light F–T and Strong F–T treatments did not alter significantly the overall nanoparticle concentrations of samples as checked by iNTA (SI Fig. S5A). DSG processing of Light F–T and Strong F–T samples revealed that the two treatments induced changes in the distribution within the gradient fractions with the fresh sample. After Light F–T treatment, we could still observe the presence of two subpopulations (Fig. 4A): one in fractions 5 to 9 (blue box, density from 1.11 to 1.31 g cm^{-3}) and another in fractions 11 and 12 (orange box, density 1.35 g cm^{-3}). Light F–T samples presented a wider distribution in lighter fractions compared to fresh samples. Notably, fraction 5 (1.11 g cm^{-3}) in Light F–T samples contained both RBC-EV markers, Band 3 and HBB, whereas fresh samples never reached this density. In fresh samples, the lighter fraction containing both Band 3 and HBB was fraction 6, with a density of 1.16 g cm^{-3} (Fig. 1C). Additionally, the HBB present in fraction 5 of the Light F–T sample was also different from the fresh sample in fraction 6. The fresh sample in fraction 6 contained both the monomeric and dimeric forms of HBB, according to the molecular weights of the bands, while Light F–T fraction 5 contained only the monomeric form of HBB. This trend was also observed in the lighter fractions of the 6-month and 1-year samples (Fig. 2B and C). It has been demonstrated that the environment can influence hemoglobin structural changes.[60] We hypothesize that, under our experimental conditions, the monomeric form of HBB could be associated with EVs in a more stable manner than the dimers. Further studies are needed to assess the topology of HBB associated with RBC-EV: if it is considered cargo or part of the RBC-EV "biomolecular corona".[57] The trend described for the Light F–T sample was even more pronounced in the Strong F–T sample. We could observe a signal of RBC-EV also in fraction 4 (density 1.09 g cm^{-3}) (Fig. 4B, blue box), and both fractions 4 and 5 contained only the monomeric form of HBB. On the other hand, the distribution in the denser fractions also shifted compared to the Light F–T and fresh samples. Fraction 11 (1.35 g cm^{-3}) was no longer populated, and both Band 3 and HBB (monomeric form) were retained only in fraction 12 (Fig. 4B, orange box). Uncropped versions of the western blot images of Light F–T and Strong F–T can be found in SI Fig. S6A and B. Notably, the DSG factions 4 and 7 of the Strong F–T sample contained intact vesicles as verified by AFM, indicating that the F–T processes did not alter the morphology of nanoparticles and that changes in DSG fractions are not due to enrichment of cellular debris (SI Fig. S5B and C).

These results suggest that both Light F–T and Strong F–T treatments reduce the heterogeneity of RBC-EV preparations in a "dose-dependent manner", where the intensity of the treatment correlates with a greater degree of change. The observed trend indicates a shift in distribution that more closely resembles the pattern seen in the 6-month sample. This shift is also reflected in iNTA measurements. In the Light F–T samples, the relative concentration of EVs in the Upper subpopulation (contrast$^{1/3}$ > 0.7) decreased from 70% to 65%, while the Lower subpopulation (contrast$^{1/3}$ < 0.7) increased from 30% to 35%, though this difference was not statistically significant compared to fresh samples (Fig. 5B, E and G). However, in the Strong F–T sample, the effect was more pronounced, with a statistically significant shift to 25% in the upper subpopulation and 75% in the lower subpopulation compared to Light F–T (Fig. 5C, F and G).

Notably, iNTA data provided quantitative confirmation of the changes observed in DSG distribution. The Strong F–T treatment altered the physico-chemical properties of the fresh samples, making their density and contrast more similar to those of 6-month stored samples. The distribution between the upper and lower populations in the 6-month and the Strong F–T samples was not statistically different, with median relative concentrations of 20% and 25% in the upper subpopulation and 80% and 75% in the lower subpopulation, respectively (Fig. 3G and 5G).

We hypothesized that F–T cycles act as an "accelerated ageing" method, reducing sample heterogeneity by mimicking the effects of long-term storage in a shorter time.

Accelerated ageing is a strategy usually applied to a wide variety of samples: synthetic microparticles[61] and nanoparticles,[62] organic[63] and synthetic[64] polymers,[65] plant seeds,[66] and pharmaceuticals.[67] Samples are subjected to different types of treatments.[67] The evaluation of the changes induced helps in the determination of the long-term effects of expected levels of stress within a shorter time[68] and to select samples with determined characteristics and performances.[66]

Size distribution is a physicochemical characteristic that can be modified after different long-term storage conditions,

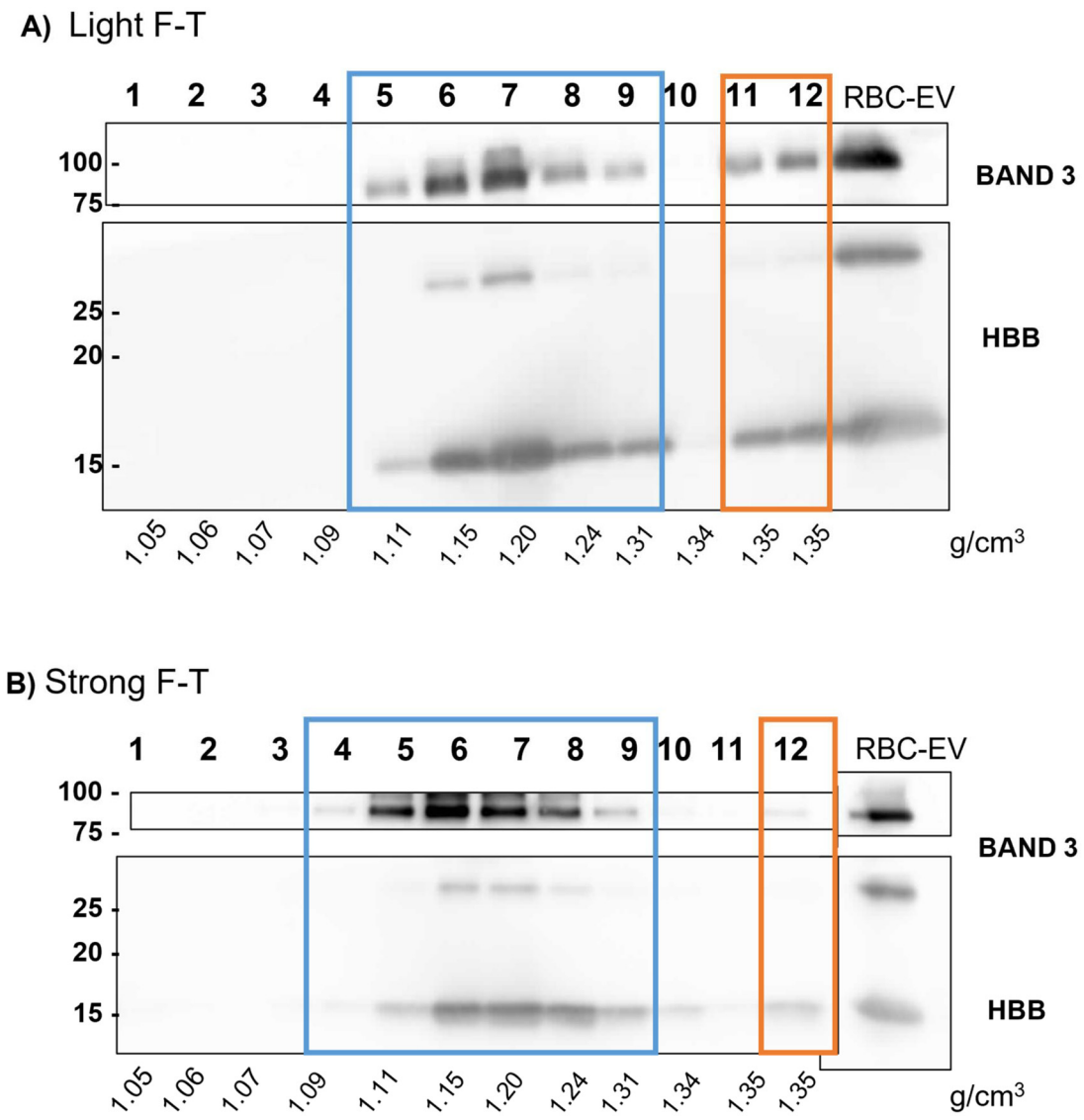

Fig. 4 Gradient distribution of RBC-EVs after freeze–thaw cycles. Equal volumes (15 μL) of each fraction for both Light freeze–thaw cycles (Light F–T, A) and Strong freeze–thaw cycles (Strong F–T, B), 30 μg of RBC-EV homogenate (RBC-EV) samples were loaded. Samples were electrophoresed on 12% SDS-PAGE gel (acrylamide/bis-acrylamide) and analyzed for the antibodies described in the figures. Uncropped WBs are available in the SI (Fig. S6). Each fraction density is indicated in g cm^{-3}. RBC-EV subpopulations with different gradient distributions are indicated in colored boxes: (A) blue box: fractions 5–9; orange box: fractions 11–12; (B) blue box: fractions 4–9; and (C) blue box: fraction 12.

both for EVs[69] and synthetic nanoparticles.[70] In addition, accelerated ageing can be applied to control this parameter in synthetic materials.[62]

Building on this, we used iNTA to investigate the differences in the size distribution of nanoparticles in the five RBC-EV samples: fresh, 6-month, 1-year, Light F–T, and Strong F–T. In the fresh sample (Fig. 3A), two distinct subpopulations – below 100 nm (30–100 nm Fig. 6A and B; purple histograms) and above 100 nm (Fig. 6A and C; green histograms) – were easily distinguishable. Using these defined size ranges, we quantified the number of EVs in all samples.

As shown in Fig. 6A, the fresh sample has a relative quantification of 0.16 for particles below 100 nm (purple histogram) and 0.84 for particles above 100 nm (green histogram). After 6 months and 1 year of storage at −80 °C, the size distribution of RBC-EVs shifted significantly. Specifically, the relative quantification of the subpopulation below 100 nm increased to 0.42 in the 6-month sample and to 0.36 in the 1-year sample, both statistically significant compared to the fresh sample (Fig. 6A and B). Consequently, the subpopulation above 100 nm decreased to 0.58 in the 6-month sample and 0.64 in the 1-year sample (Fig. 6C). These results indicate that long-term storage alters the relative size distribution of the RBC-EV nanoparticles, leading to an increased proportion of smaller particles.

This trend is further supported by the accelerated ageing process, as the Strong F–T sample exhibited a statistically significant increase in the relative quantification of particles below 100 nm compared to the fresh and Light F–T samples.

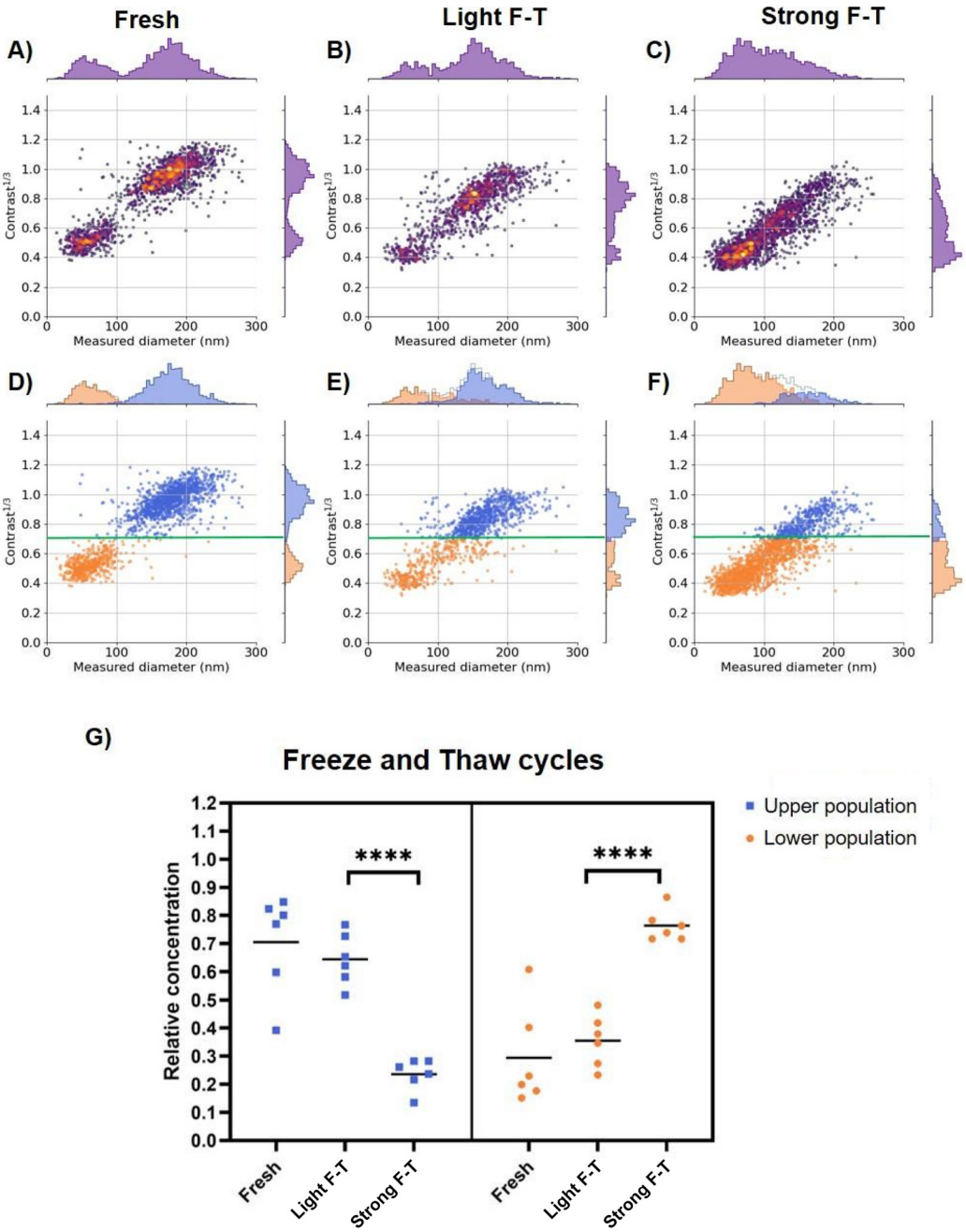

Fig. 5 Size distribution and contrast evaluation of RBC-EVs after freeze–thaw cycles. Analysis by iNTA of fresh (A), Light F–T (B), and Strong F–T (C) samples. Images represent size distribution (*x*-axis) and contrast (*y*-axis) of the nanoparticles. Nanoparticle subpopulations grouped for their contrast in fresh (D), Light F–T (E), and Strong F–T (F) samples. The green line represents a contrast$^{1/3}$ value of 0.7. Nanoparticle distribution determined for contrast$^{1/3}$ >0.7 (blue dots, upper population) or <0.7 (orange dots, lower population). (G) Relative concentration of nanoparticles present in the upper (contrast$^{1/3}$ >0.7) and lower (contrast$^{1/3}$ <0.7) populations for fresh, 6-month, and 1-year samples. Statistical analysis using Student's *t*-test: ****p value < 0.0001.

Specifically, the proportion rose from 0.16 in the fresh sample and 0.14 in the Light F–T sample to 0.37 in the Strong F–T sample (Fig. 6A and B). Taken together, these data demonstrate that after the Strong F–T treatment, RBC-EV physicochemical characteristics resemble those of the sample stored for 6 months at −80 °C.

This effect has been described in liposome synthesis where extrusion, sonication, or ultrasound[71] are used to break up multilamellar lipid vesicles and reduce liposome size.[72] As for density and contrast, we hypothesize that freezing processing could perturb RBC-EVs, and at room temperature, the vesicles tend to reform at a smaller size. Freezing typically leads to the

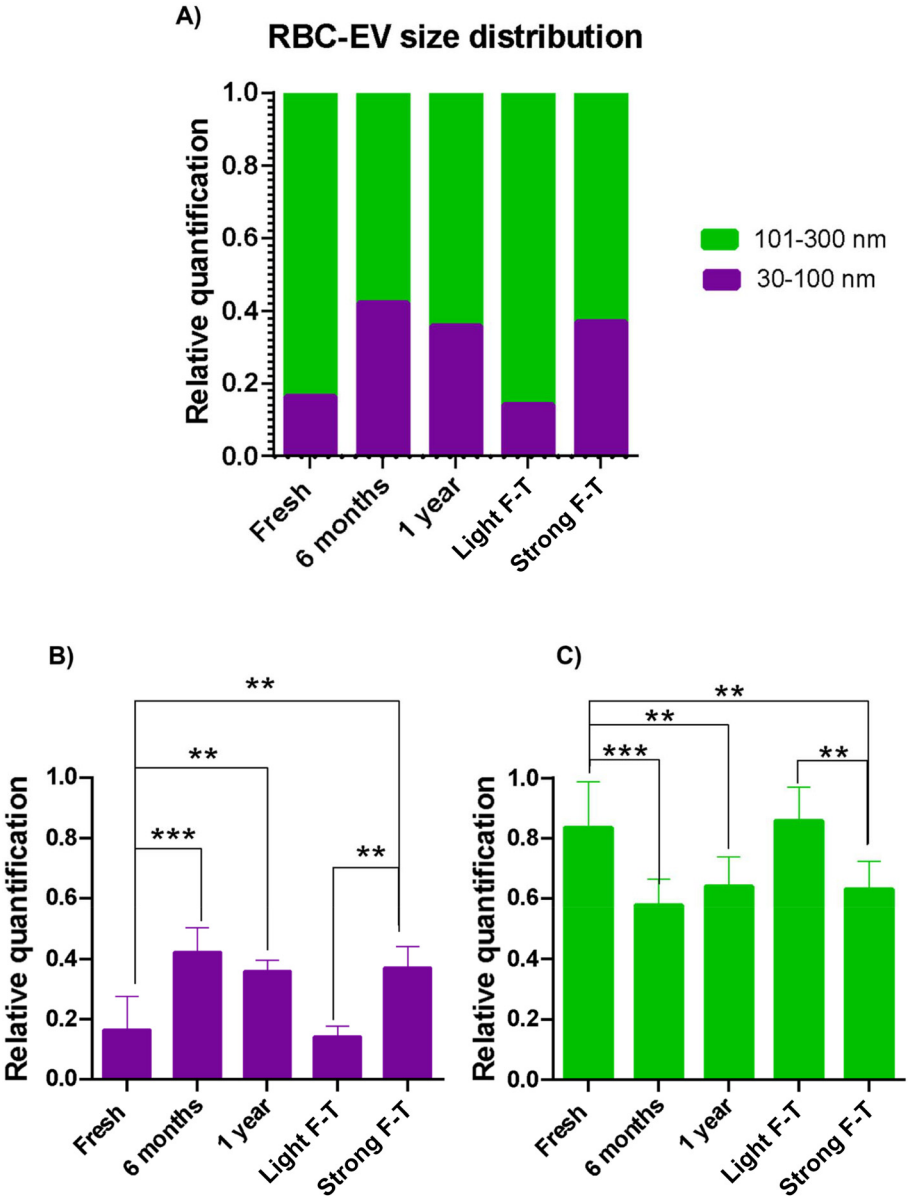

Fig. 6 Size distribution evaluation of RBC-EVs after different storage times and F–T cycles. Characterization of RBC-EVs with iNTA. (A) Relative quantification of nanoparticles with a diameter ranging from 30 to 100 nm (purple bars) and from 101 to 300 nm (green bars). (B) Statistical analysis (ANOVA test) of changes in the size distribution for nanoparticles from 30 to 100 nm, (C) Statistical analysis of nanoparticles from 101 to 300 nm. ** p value ≤ 0.01; *** p value ≤ 0.001.

formation of ice crystals, which can physically rupture cellular membranes or nanoparticles,[73] including vesicles such as RBC-EVs. This mechanical stress could result in the breakdown of larger vesicles or a reduction in their size. Upon F–T processing, the two EV subpopulations might mix and reassemble in a more compact form, leading to a reduction in their size.[74] This process may be a stochastic one, as the phospholipid bilayer could reform spontaneously, potentially driven by its amphiphilic nature and geometry, associating in an aqueous environment to form membranes[75] rather than relying on active molecular machinery (*i.e.*, the endosomal sorting complex required for transport (ESCRT) machinery for EV biogenesis)[76] responsible for vesicle formation. Compared to their original state, this reorganization could result in smaller and less dense particles, generated by random encapsulation events.[77] Moreover, the results observed in this study are consistent with findings in other nanoparticle systems, including other types of extracellular vesicles (*e.g.*, plasma EVs),[69,73] where freezing and thawing can significantly alter size distribution and lead to a narrowing of the size range. The observed trend in RBC-EVs suggests that the size reduction and narrowing of size distribution over prolonged storage or freeze–thaw cycles might be a general phenomenon that could affect various types of EVs or lipid-based nanoparticles.

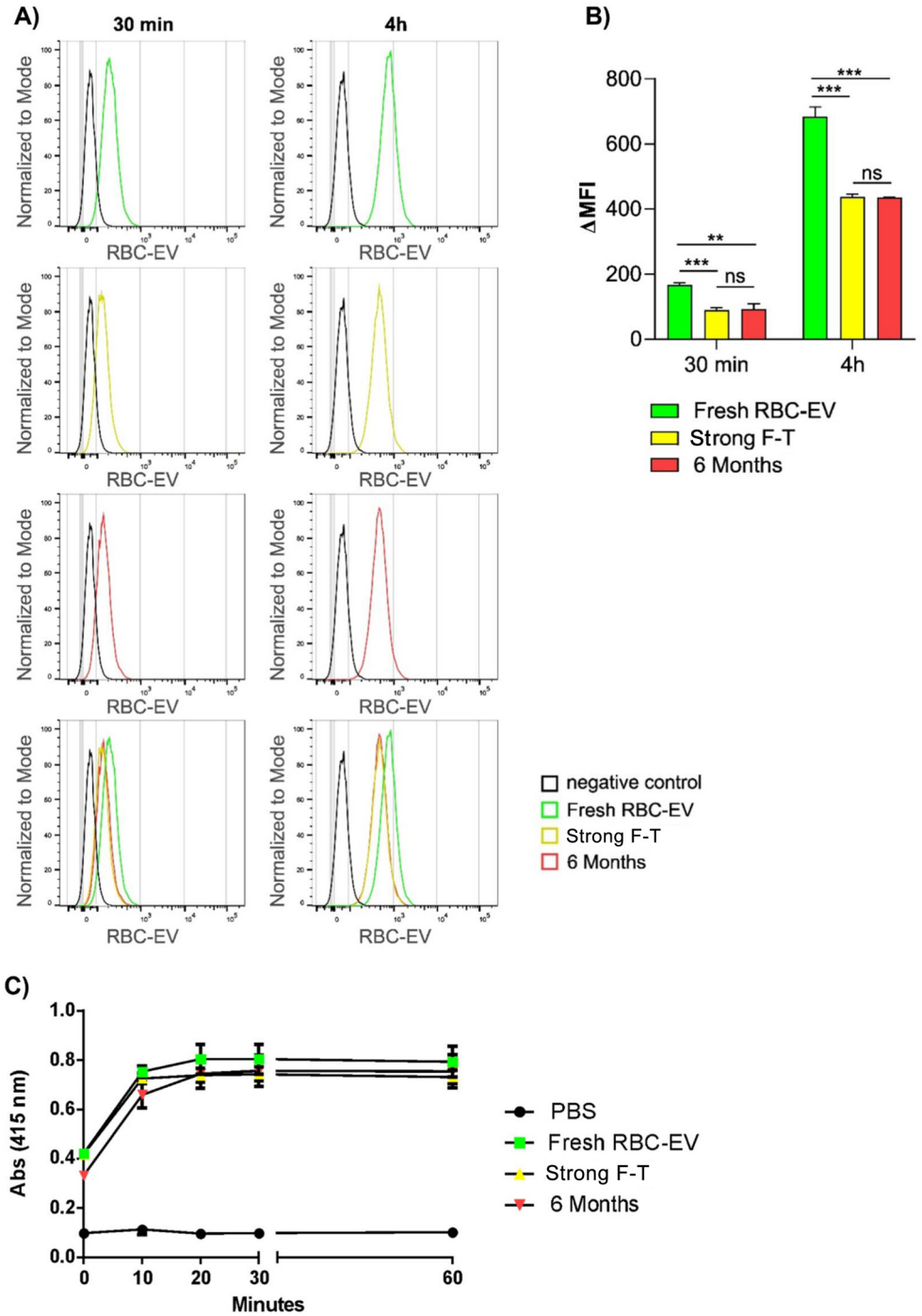

Fig. 7 RBC-EV preparations: biological activity. (A) Flow cytometry analysis of RBC-EV uptake by MDA-MB-231 cells. Fresh (green), Strong F–T (yellow) and 6-month (red) samples stained with MemGlow™ 488 fluorescent dye and incubated with MDA-MB-231 cells for either 30 min or 4 h. Cells were detached with trypsin to obtain single-cell suspensions. Representative histograms are shown for both 30 min and 4 h incubation. The fluorescence signal is compared to a negative control consisting of untreated cells. An overlay of all the experimental points is provided for both time points. (B) Bars represent mean ± standard deviation of median fluorescence intensity (MFI) – MFI of the negative control (ΔMFI), $n = 3$, $^{**}p < 0.01$, $^{***}p < 0.001$, and ns = not significant; Student's t test. (C) Acetylcholinesterase enzymatic activity measured after incubation of fresh (green square), 6-month (red downward triangle) and Strong F–T (yellow upward triangle) samples with 1.25 mM acetylthiocholine and 0.1 mM 5,5′-dithiobis(2-nitrobenzoic acid) in a final volume of 1 ml. An equal volume of PBS was used as a negative control (black dots), the incubation was carried out at 37 °C, and the change in absorbance at 415 nm was measured after 0, 10, 20, 30, and 60 min.

In conclusion, by measuring density, contrast[1/3] and size distribution, we showed that Strong F–T treatment produces RBC-EVs with properties resembling those of long-term stored samples. This approach may be useful for studying storage-related changes or for selecting samples that mimic long-term stored EVs.

3.4 Accelerated ageing influences RBC-EV cellular uptake but not their surface protein activity

It has been demonstrated that the biophysical and biochemical properties of biogenic[58,78] and synthetic nanoparticles[79,80] influence their biological activities. In order to analyze if the modifications induced in RBC-EV preparations after prolonged storage and accelerated ageing could affect their interaction with cells and surface protein activity, we analyzed their cellular uptake and enzymatic activity. To assess their interaction with cells, we incubated equal particle numbers of fluorescently labelled RBC-EV from fresh, 6-month, and Strong F–T with triple-negative breast cancer MDA-MB-231 cells for 30 min and 4 h. Indeed, we previously demonstrated significant uptake of RBC-EVs by this cell line.[8] Flow cytometry was performed to quantify RBC-EV uptake. Analyses revealed that fresh RBC-EVs were internalized by MDA-MB-231 cells to a greater extent than 6-month and Strong F–T RBC-EVs at both shorter (30 min) and extended (4 h) time points. No significant differences were observed between the uptake of 6-month and Strong F–T EVs, thus suggesting that the protocol including freeze–thaw cycles effectively mimics the prolonged storage at −80 °C (Fig. 7A and B). Any nonspecific fluorescent signals arising from possibly increased cell autofluorescence due to EV internalization or from unbound MemGlow™ 488 fluorescent dye can be excluded: indeed, the signals from the aforementioned two experimental controls perfectly overlay the signals of the negative control, *i.e.*, untreated cells (SI Fig. S7). It is worth noting that after 4 h of incubation, the positivity of cells increases four times, regardless of the experimental conditions (Fig. 7B). These results indicated that narrowing the heterogeneity of RBC-EVs can influence their interaction with target cells.

In addition, we aimed to verify whether prolonged storage and F–T cycles affect the surface proteins present on the external membrane of RBC-EVs. To test this, we analyzed the activity of acetylcholinesterase, a glycoprotein with enzymatic activity[81] present on the surface of red blood cells and thus on RBC-EVs,[82] in fresh, 6-month, and Strong F–T cycle samples. As shown in Fig. 7C and SI Fig. S8, there were no significant differences in the enzymatic activity among the analyzed samples, indicating that the biological activity of enzymes present on the surface of the RBC-EVs is altered neither by prolonged storage nor by Strong F–T cycles. This finding suggests two important points: (1) the reduced cellular uptake of stored EVs is likely due to factors other than surface enzyme degradation and (2) the preservation of AChE activity highlights the robustness of the RBC-EV membrane's functional integrity. However, while AChE activity was maintained, further studies should analyze other surface proteins for a comprehensive evaluation and comparison with other proteins that could be either transmembrane or part of the biomolecular corona.[8,83,84]

4. Conclusions

EVs are diverse nanoparticles with large heterogeneity in size and molecular composition. Although this heterogeneity provides high diagnostic value for liquid biopsy and confers many exploitable functions for therapeutic applications in cancer detection, wound healing and neurodegenerative and cardiovascular diseases, it has also impeded their clinical translation. Heterogeneity, therefore, acts as a double-edged sword in the development of EV-based applications.[85,86]

The development of EVs as advanced biomaterials is affected by this complexity, posing several bioprocessing challenges.[26] New and standardized technologies, informed by a better understanding of their physicochemical landscape, are required for their translation into starting materials for biomedical technologies and marketable products.[26]

In this study, we developed an "accelerated-ageing" method based on freeze–thaw cycles that drives RBC-EV samples into highly homogeneous preparations in terms of density, size distribution, and biological activity, effectively mimicking the biophysical characteristics of preparations stored for 6 months at −80 °C. Our findings highlight that long-term storage effectively reduces RBC-EV heterogeneity, leading to a shift towards smaller and less dense particle subpopulations. Furthermore, our experiments showed that the reduced heterogeneity and smaller size of RBC-EVs, induced by either long-term storage or F–T cycles, impacted their cellular uptake in a similar way. This suggests that the subpopulation present in fresh RBC-EVs that is able to afford the highest uptake yield is the most unstable under different storage conditions.

In conclusion, freezing-induced accelerated ageing provides a robust pathway toward standardized and optimized RBC-EV preparations. This method represents a critical step in translating these vesicles into reliable building blocks for biomaterial, bioengineering, and therapeutic applications. The full realization of this potential, encompassing applications like targeted drug delivery, now hinges on future studies with expanded donor cohorts (spanning different ages, genders and health conditions). Moreover, dedicated application-focused testing such as drug encapsulation efficiency studies, release kinetic assessments, and comparisons with other stabilization techniques (*e.g.*, lyophilization with or without additives) will be key to optimizing RBC-EV formulations for translational and therapeutic applications.

Overall, our results underscore the importance of considering storage and processing conditions when preparing RBC-EVs for research or clinical applications, as these factors can significantly alter their properties and behavior.[89] The F–T cycle method offers a valuable tool for simulating long-term storage effects, which is crucial for drug development.

The observed phenomena could be attributed to both extrinsic and intrinsic stochastic effects. Stochastic reactions can be simulated *in silico* by considering the number of molecules in a reacting system (*e.g.*, the aqueous vesicle core) and calculating the probability of any possible reaction taking place accordingly. This opens a new perspective for using our model in "Synthetic Biology"[87,88] experiments, representing concrete steps towards the identification of key active biomolecules/properties that determine EV mechanisms of action across different EV subtypes.

Author contributions

Conceptualization: LP, MR and AR; data curation: LP, MR, VM, ST, SJ, AK, ELM, AM, and AZ; funding acquisition: PB and AR; investigation: LP, MR, ACB, SCG, PB, and AR; methodology: LP, MR, SJ, AK, and VS; writing – original draft: LP and AR; and writing – review & editing: all authors.

Conflicts of interest

There are no conflicts to declare.

Data availability

Data supporting this article have been included in the main text and as part of the supplementary information (SI). Supplementary information is available. See DOI: https://doi.org/10.1039/d5bm01349f.

Acknowledgements

This work was supported by Project CN3 PNRR – Centro Nazionale sullo sviluppo di terapia genica e farmaci con tecnologia a RNA and by the project Organocar, funded by the Heal Italia Project, led by Spoke 5 (Next Generation Therapeutics) – University of Milan-Bicocca.

The authors would like to thank the "Labion Lab" of the IRCCS Fondazione Don Carlo Gnocchi ONLUS, Milan, Italy, for NTA measurements. Table of Content created in BioRender. Radeghieri, A. (2025) https://BioRender.com/32vlv4s.

References

1 C. Théry, K. W. Witwer, E. Aikawa, M. J. Alcaraz, J. D. Anderson, R. Andriantsitohaina, *et al.*, Minimal information for studies of extracellular vesicles 2018 (MISEV2018): a position statement of the International Society for Extracellular Vesicles and update of the MISEV2014 guidelines, *J. Extracell. Vesicles*, 2018, **7**(1), 1535750.
2 I. Petraroia, P. Ghidotti, G. Bertolini, F. Pontis, L. Roz, M. Balsamo, *et al.*, Extracellular vesicles from subjects with COPD modulate cancer initiating cells phenotype through HIF-1α shuttling, *Cell Death Dis.*, 2023, **14**(10), 681.
3 N. Raab-Traub and D. P. Dittmer, Viral effects on the content and function of extracellular vesicles, *Nat. Rev. Microbiol.*, 2017, **15**(9), 559–572.
4 R. Kalluri and V. S. LeBleu, The biology, function, and biomedical applications of exosomes, *Science*, 2020, **367**(6478), eaau6977.
5 S. K. Kumar and M. V. Sasidhar, Recent Trends in the Use of Small Extracellular Vesicles as Optimal Drug Delivery Vehicles in Oncology, *Mol. Pharm.*, 2023, **20**(8), 3829–3842.
6 I. K. Herrmann, M. J. A. Wood and G. Fuhrmann, Extracellular vesicles as a next-generation drug delivery platform, *Nat. Nanotechnol.*, 2021, **16**(7), 748–759.
7 C. T. Pham, X. Zhang, A. Lam and M. T. Le, Red blood cell extracellular vesicles as robust carriers of RNA-based therapeutics, *Cell Stress*, 2018, **2**(9), 239–241.
8 A. Musicò, R. Zenatelli, M. Romano, A. Zendrini, S. Alacqua, S. Tassoni, *et al.*, Surface functionalization of extracellular vesicle nanoparticles with antibodies: a first study on the protein corona "variable", *Nanoscale Adv.*, 2023, **5**(18), 4703–4717.
9 T. C. Pham, M. K. Jayasinghe, T. T. Pham, Y. Yang, L. Wei, W. M. Usman, *et al.*, Covalent conjugation of extracellular vesicles with peptides and nanobodies for targeted therapeutic delivery, *J. Extracell. Vesicles*, 2021, **10**(4), e12057.
10 T. T. Pham, H. Chen, P. H. D. Nguyen, M. K. Jayasinghe, A. H. Le and M. T. Le, Endosomal escape of nucleic acids from extracellular vesicles mediates functional therapeutic delivery, *Pharmacol. Res.*, 2023, **188**, 106665.
11 P. H. D. Nguyen, M. K. Jayasinghe, A. H. Le, B. Peng and M. T. N. Le, Advances in Drug Delivery Systems Based on Red Blood Cells and Their Membrane-Derived Nanoparticles, *ACS Nano*, 2023, **17**(6), 5187–5210.
12 L. Repsold and A. M. Joubert, Eryptosis: An Erythrocyte's Suicidal Type of Cell Death, *BioMed Res. Int.*, 2018, **2018**, 9405617.
13 R. A. Dodson, T. R. Hinds and F. F. Vincenzi, Effects of Calcium and A23187 on Deformability and Volume of Human Red Blood Cells, *Blood Cells*, 1987, **12**(3), 555–564.
14 S. Hasse, A. C. Duchez, P. Fortin, E. Boilard and S. G. Bourgoin, Interplay between LPA2 and LPA3 in LPA-mediated phosphatidylserine cell surface exposure and extracellular vesicles release by erythrocytes, *Biochem. Pharmacol.*, 2021, **192**, 114667.
15 D. B. Nguyen, T. B. Thuy Ly, M. C. Wesseling, M. Hittinger, A. Torge, A. Devitt, *et al.*, Characterization of microvesicles released from human red blood cells, *Cell. Physiol. Biochem.*, 2016, **38**(3), 1085–1099.
16 M. Ebeyer-Masotta, T. Eichhorn, M. B. Fischer and V. Weber, Impact of production methods and storage conditions on extracellular vesicles in packed red blood cells and platelet concentrates, *Transfus. Apher. Sci.*, 2024, **63**(2), 103891.

17 C. Gamonet, M. Desmarets, G. Mourey, S. Biichle, S. Aupet, C. Laheurte, *et al.*, Processing methods and storage duration impact extracellular vesicle counts in red blood cell units, *Blood Adv.*, 2020, **4**(21), 5527–5539.
18 W. M. Usman, T. C. Pham, Y. Y. Kwok, L. T. Vu, V. Ma, B. Peng, *et al.*, Efficient RNA drug delivery using red blood cell extracellular vesicles, *Nat. Commun.*, 2018, **9**(1), 2359.
19 M. Prudent, D. Crettaz, J. Delobel, J. Seghatchian, J. D. Tissot and N. Lion, Differences between calcium-stimulated and storage-induced erythrocyte-derived microvesicles, *Transfus. Apher. Sci.*, 2015, **53**(2), 153–158.
20 U. Salzer, R. Zhu, M. Luten, H. Isobe, V. Pastushenko, T. Perkmann, *et al.*, Vesicles generated during storage of red cells are rich in the lipid raft marker stomatin, *Transfusion*, 2008, **48**(3), 451–462.
21 G. P. de Oliveira, J. A. Welsh, B. Pinckney, C. C. Palu, S. Lu, A. Zimmerman, *et al.*, Human red blood cells release microvesicles with distinct sizes and protein composition that alter neutrophil phagocytosis, *J. Extracell. Biol.*, 2023, **2**(11), e107.
22 G. D. Kusuma, M. Barabadi, J. L. Tan, D. A. V. Morton, J. E. Frith and R. Lim, To Protect and to Preserve: Novel Preservation Strategies for Extracellular Vesicles, *Front. Pharmacol.*, 2018, **9**, 1199.
23 R. J. Almizraq, J. Seghatchian, J. L. Holovati and J. P. Acker, Extracellular vesicle characteristics in stored red blood cell concentrates are influenced by the method of detection, *Transfus. Apher. Sci.*, 2017, **56**(2), 254–260.
24 T. Bebesi, D. Kitka, A. Gaál, I. C. Szigyártó, R. Deák, T. Beke-Somfai, *et al.*, Storage conditions determine the characteristics of red blood cell derived extracellular vesicles, *Sci. Rep.*, 2022, **12**(1), 977.
25 M. Straat, A. N. Böing, A. Tuip-De Boer, R. Nieuwland and N. P. Juffermans, Extracellular Vesicles from Red Blood Cell Products Induce a Strong Pro-Inflammatory Host Response, Dependent on Both Numbers and Storage Duration, *Transfus. Med. Hemother.*, 2016, **43**(4), 302–305.
26 L. Paolini, M. Monguió-Tortajada, M. Costa, F. Antenucci, M. Barilani, M. Clos-Sansalvador, *et al.*, Large-scale production of extracellular vesicles: Report on the "massivEVs", ISEV workshop, *J. Extracell. Biol.*, 2022, **1**(10), e63.
27 B. C. Nelson, S. Maragh, I. C. Ghiran, J. C. Jones, P. C. DeRose, E. Elsheikh, *et al.*, Measurement and standardization challenges for extracellular vesicle therapeutic delivery vectors, *Nanomedicine*, 2020, **15**(22), 2149–2170.
28 ICH Q1A(R2) Stability Testing of New Drug Substances and Products, *Food Drug Adm.*, 2003, https://www.fda.gov/regulatory-information/search-fda-guidance-documents/q1ar2-stability-testing-new-drug-substances-and-products.
29 *ICH Q1A (R2) Stability testing of new drug substances and drug products – Scientific guideline*. European Medicines Agency (EMA), 2003, https://www.ema.Europa.eu/en/ich-q1a-r2-stability-testing-new-drug-substances-drug-products-scientific-guideline#current-effective-version-8899.
30 J. A. Saugstad, T. A. Lusardi, K. R. Van Keuren-Jensen, J. I. Phillips, B. Lind, C. A. Harrington, *et al.*, Analysis of extracellular RNA in cerebrospinal fluid, *J. Extracell. Vesicles*, 2017, **6**(1), 1317577.
31 Y. Tian, M. Gong, Y. Hu, H. Liu, W. Zhang, M. Zhang, *et al.*, Quality and efficiency assessment of six extracellular vesicle isolation methods by nano-flow cytometry, *J. Extracell. Vesicles*, 2020, **9**(1), 1697028.
32 A. Gori, A. Romanato, G. Bergamaschi, A. Strada, P. Gagni, R. Frigerio, *et al.*, Membrane-binding peptides for extracellular vesicles on-chip analysis, *J. Extracell. Vesicles*, 2020, **9**(1), 1751428.
33 A. Ridolfi, M. Brucale, C. Montis, L. Caselli, L. Paolini, A. Borup, *et al.*, AFM-Based High-Throughput Nanomechanical Screening of Single Extracellular Vesicles, *Anal. Chem.*, 2020, **92**(15), 10274–10282.
34 G. Raposo and W. Stoorvogel, Extracellular vesicles: exosomes, microvesicles, and friends, *J. Cell Biol.*, 2013, **200**(4), 373–383.
35 C. Carlomagno, C. Giannasi, S. Niada, M. Bedoni, A. Gualerzi and A. T. Brini, Raman Fingerprint of Extracellular Vesicles and Conditioned Media for the Reproducibility Assessment of Cell-Free Therapeutics, *Front. Bioeng. Biotechnol.*, 2021, **9**, 640617.
36 L. Paolini, S. Federici, G. Consoli, D. Arceri, A. Radeghieri, I. Alessandri, *et al.*, Fourier-transform Infrared (FT-IR) spectroscopy fingerprints subpopulations of extracellular vesicles of different sizes and cellular origin, *J. Extracell. Vesicles*, 2020, **9**(1), 1741174.
37 A. Koponen, E. Kerkelä, T. Rojalin, E. Lázaro-Ibáñez, T. Suutari, H. O. Saari, *et al.*, Label-free characterization and real-time monitoring of cell uptake of extracellular vesicles, *Biosens. Bioelectron.*, 2020, **168**, 112510.
38 A. D. Kashkanova, M. Blessing, A. Gemeinhardt, D. Soulat and V. Sandoghdar, Precision size and refractive index analysis of weakly scattering nanoparticles in polydispersions, *Nat. Methods*, 2022, **19**(5), 586–593.
39 A. D. Kashkanova, M. Blessing, M. Reischke, J. O. Baur, A. S. Baur, V. Sandoghdar, *et al.*, Label-free discrimination of extracellular vesicles from large lipoproteins, *J. Extracell. Vesicles*, 2023, **12**(8), e12348.
40 J. Van Deun, P. Mestdagh, P. Agostinis, Ö. Akay, S. Anand, J. Anckaert, *et al.*, EV-TRACK: transparent reporting, centralizing knowledge in extracellular vesicle research, *Nat. Methods*, 2017, **14**(3), 228–232.
41 I. Grossi, A. Radeghieri, L. Paolini, V. Porrini, A. Pilotto, A. Padovani, *et al.*, MicroRNA-34a-5p expression in the plasma and in its extracellular vesicle fractions in subjects with Parkinson's disease: An exploratory study, *Int. J. Mol. Med.*, 2020, **47**(2), 533–546.
42 A. Radeghieri, S. Alacqua, A. Zendrini, V. Previcini, F. Todaro, G. Martini, *et al.*, Active antithrombin glycoforms are selectively physiosorbed on plasma extracellular vesicles, *J. Extracell. Biol.*, 2022, **1**(9), e57.
43 L. Paolini, A. Radeghieri, S. Civini, L. Caimi and D. Ricotta, The Epsilon Hinge-Ear Region Regulates Membrane Localization of the AP-4 Complex, *Traffic*, 2011, **12**(11), 1604–1619.

44 G. Di Noto, E. Cimpoies, A. Dossi, L. Paolini, A. Radeghieri, L. Caimi, *et al.*, Polyclonal versus monoclonal immunoglobulin-free light chains quantification, *Ann. Clin. Biochem. Int. J. Lab. Med.*, 2015, **52**(3), 327–336.
45 G. Alvisi, L. Paolini, A. Contarini, C. Zambarda, V. Di Antonio, A. Colosini, *et al.*, Intersectin goes nuclear: secret life of an endocytic protein, *Biochem. J.*, 2018, **475**(8), 1455–1472.
46 A. Salvi, M. Vezzoli, S. Busatto, L. Paolini, T. Faranda, E. Abeni, *et al.*, Analysis of a nanoparticle-enriched fraction of plasma reveals miRNA candidates for Down syndrome pathogenesis, *Int. J. Mol. Med.*, 2019, **2**, 768.
47 J. S. Shah, P. S. Soon and D. J. Marsh, Comparison of Methodologies to Detect Low Levels of Hemolysis in Serum for Accurate Assessment of Serum microRNAs. Janigro D, editor, *PLoS One*, 2016, **11**(4), e0153200.
48 D. Maiolo, L. Paolini, G. Di Noto, A. Zendrini, D. Berti, P. Bergese, *et al.*, Colorimetric Nanoplasmonic Assay To Determine Purity and Titrate Extracellular Vesicles, *Anal. Chem.*, 2015, **87**(8), 4168–4176.
49 A. Zendrini, L. Paolini, S. Busatto, A. Radeghieri, M. Romano, M. H. M. Wauben, *et al.*, Augmented COlorimetric NANoplasmonic (CONAN) Method for Grading Purity and Determine Concentration of EV Microliter Volume Solutions, *Front. Bioeng. Biotechnol.*, 2020, **7**, 452.
50 A. Borup, A. T. Boysen, A. Ridolfi, M. Brucale, F. Valle, L. Paolini, *et al.*, Comparison of separation methods for immunomodulatory extracellular vesicles from helminths, *J. Extracell. Biol.*, 2022, **1**(5), e41.
51 A. D. Kashkanova, D. Albrecht, M. Küppers, M. Blessing and V. Sandoghdar, Measuring Concentration of Nanoparticles in Polydisperse Mixtures Using Interferometric Nanoparticle Tracking Analysis, *ACS Nano*, 2024, **18**(29), 19161–19168.
52 I. K. Ho and G. L. Ellman, Triton solubilized acetylcholinesterase of brain, *J. Neurochem.*, 1969, **16**(11), 1505–1513.
53 A. Savina, M. Vidal and M. I. Colombo, The exosome pathway in K562 cells is regulated by Rab11, *J. Cell Sci.*, 2002, **115**(12), 2505–2515.
54 J. A. Welsh, D. C. I. Goberdhan, L. O'Driscoll, E. I. Buzas, C. Blenkiron, B. Bussolati, *et al.*, Minimal information for studies of extracellular vesicles (MISEV2023): From basic to advanced approaches, *J. Extracell. Vesicles*, 2024, **13**(2), e12404.
55 F. Lucien, D. Gustafson, M. Lenassi, B. Li, J. J. Teske, E. Boilard, *et al.*, MIBlood-EV: Minimal information to enhance the quality and reproducibility of blood extracellular vesicle research, *J. Extracell. Vesicles*, 2023, **12**(12), e12385.
56 A. Gori, R. Frigerio, P. Gagni, J. Burrello, S. Panella, A. Raimondi, *et al.*, Addressing Heterogeneity in Direct Analysis of Extracellular Vesicles and Their Analogs by Membrane Sensing Peptides as Pan-Vesicular Affinity Probes, *Adv. Sci.*, 2024, **11**(29), 2400533.
57 A. Musicò, A. Zendrini, S. Gimenez Reyes, V. Mangolini, L. Paolini, M. Romano, *et al.*, Extracellular vesicles of different cellular origin feature distinct biomolecular corona dynamics, *Nanoscale Horiz.*, 2025, **10**(1), 104–112.
58 F. Caponnetto, I. Manini, M. Skrap, T. Palmai-Pallag, C. Di Loreto, A. P. Beltrami, *et al.*, Size-dependent cellular uptake of exosomes, *Nanomedicine*, 2017, **13**(3), 1011–1020.
59 V. Mangolini, A. Radeghieri, S. Piva, S. Cattaneo, M. Brucale, F. Valle, *et al.*, Universal protocol to separate and compare Extracellular Vesicles from human plasma and skeletal muscle biopsy, *bioRxiv*, 2025, preprint, DOI: 10.1101/2024.02.19.580950v2.
60 Y. X. Huang, Z. J. Wu, B. T. Huang and M. Luo, Pathway and Mechanism of pH Dependent Human Hemoglobin Tetramer-Dimer-Monomer Dissociations, *PLoS One*, 2013, **8**(11), e81708.
61 X. Cheng, S. Wang, X. Zhang, M. S. Iqbal, Z. Yang, Y. Xi, *et al.*, Accelerated ageing behavior of degradable and non-degradable microplastics via advanced oxidation and their adsorption characteristics towards tetracycline, *Ecotoxicol. Environ. Saf.*, 2024, **284**, 116864.
62 I. A. Shuklov, V. F. Toknova, A. A. Lizunova and V. F. Razumov, Controlled ageing of PbS colloidal quantum dots under mild conditions, *Mater. Today Chem.*, 2020, **18**, 100357.
63 P. Calvini and A. Gorassini, On the Rate of Paper Degradation: Lessons From the Past, *Restaurator*, 2006, **27**(4), 275–290.
64 L. Fambri, R. Caria, F. Atzori, R. Ceccato and D. Lorenzi, *et al.*, *Controlled Ageing and Degradation of Selected Plastics in Marine Environment: 12 Months of Follow-up*, in *Proceedings of the 2nd International Conference on Microplastic Pollution in the Mediterranean Sea*, ed. M. Cocca, E. Di Pace, M.E Errico, G. Gentile, A. Montarsolo and R. Mossotti, Springer International Publishing, Cham, 2020, pp. 89–100.
65 D. Kockott, New method for accelerated testing of the ageing behavior of polymeric materials as a function of radiation and temperature, *Polym. Test.*, 2022, **110**, 107550.
66 E. Fenollosa, L. Jené and S. Munné-Bosch, A rapid and sensitive method to assess seed longevity through accelerated ageing in an invasive plant species, *Plant Methods*, 2020, **16**(1), 64.
67 K. C. Waterman and R. C. Adami, Accelerated ageing: prediction of chemical stability of pharmaceuticals, *Int. J. Pharm.*, 2005, **293**(1–2), 101–125.
68 X. Zou, T. Uesaka and N. Gurnagul, Prediction of paper permanence by accelerated ageing I. Kinetic analysis of the ageing process, *Cellulose*, 1996, **3**(1), 243–267.
69 S. Gelibter, G. Marostica, A. Mandelli, S. Siciliani, P. Podini, A. Finardi, *et al.*, The impact of storage on extracellular vesicles: A systematic study, *J. Extracell. Vesicles*, 2022, **11**(2), e12162.
70 J. Gubicza, J. L. Lábár, L. M. Quynh, N. H. Nam and N. H. Luong, Evolution of size and shape of gold nanoparticles during long-time ageing, *Mater. Chem. Phys.*, 2013, **138**(2), 449–453.

71 X. Huang, R. Caddell, B. Yu, S. Xu, T. Theobald, L. J. Lee, *et al.*, Ultrasound-enhanced microfluidic synthesis of liposomes, *Anticancer Res.*, 2010, **30**(2), 463–466.
72 J. S. Yun, S. A. Hwangbo and Y. G. Jeong, Preparation of Uniform Nano Liposomes Using Focused Ultrasonic Technology, *Nanomaterials*, 2023, **13**(19), 2618.
73 A. Sivanantham and Y. Jin, Impact of Storage Conditions on EV Integrity/Surface Markers and Cargos, *Life*, 2022, **12**(5), 697.
74 P. Grosfils and P. Losada-Pérez, Kinetic control of liposome size by direct lipid transfer, *J. Colloid Interface Sci.*, 2023, **652**, 1381–1393.
75 S. Svetina and B. Zeks, Shape behavior of lipid vesicles as the basis of some cellular processes, *Anat. Rec.*, 2002, **268**(3), 215–225.
76 S. L. N. Maas, X. O. Breakefield and A. M. Weaver, Extracellular Vesicles: Unique Intercellular Delivery Vehicles, *Trends Cell Biol.*, 2017, **27**(3), 172–188.
77 E. Altamura, P. Carrara, F. D'Angelo, F. Mavelli and P. Stano, Extrinsic stochastic factors (solute partition) in gene expression inside lipid vesicles and lipid-stabilized water-in-oil droplets: a review, *Synth. Biol.*, 2018, **3**(1), ysy011.
78 X. Wang, Z. Zhang, Y. Qi, Z. Zhang, Y. Zhang, K. Meng, *et al.*, Study of the uptake mechanism of two small extracellular vesicle subtypes by granulosa cells, *Anim. Reprod. Sci.*, 2024, **270**, 107576.
79 A. U. Andar, R. R. Hood, W. N. Vreeland, D. L. Devoe and P. W. Swaan, Microfluidic preparation of liposomes to determine particle size influence on cellular uptake mechanisms, *Pharm. Res.*, 2014, **31**(2), 401–413.
80 P. Jurney, R. Agarwal, V. Singh, D. Choi, K. Roy, S. V. Sreenivasan, *et al.*, Unique size and shape-dependent uptake behaviors of non-spherical nanoparticles by endothelial cells due to a shearing flow, *J. Control Release*, 2017, **245**, 170–176.
81 G. Daniels, Functions of red cell surface proteins, *Vox Sang.*, 2007, **93**(4), 331–340.
82 Z. Liao, L. M. Jaular, E. Soueidi, M. Jouve, D. C. Muth, T. H. Schøyen, *et al.*, Acetylcholinesterase is not a generic marker of extracellular vesicles, *J. Extracell. Vesicles*, 2019, **8**(1), 1628592.
83 E. Á. Tóth, L. Turiák, T. Visnovitz, C. Cserép, A. Mázló, B. W. Sódar, *et al.*, Formation of a protein corona on the surface of extracellular vesicles in blood plasma, *J. Extracell. Vesicles*, 2021, **10**(11), e12140.
84 S. Tassoni, P. Bergese and A. Radeghieri, The extracellular vesicle biomolecular corona: current insights and diagnostic potential, *Nanomedicine*, 2025, **20**(16), 2013–2021.
85 R. P. Carney, R. R. Mizenko, B. T. Bozkurt, N. Lowe, T. Henson, A. Arizzi, *et al.*, Harnessing extracellular vesicle heterogeneity for diagnostic and therapeutic applications, *Nat. Nanotechnol.*, 2025, **20**(1), 14–25.
86 M. Manno, A. Bongiovanni, L. Margolis, P. Bergese and P. Arosio, The physico-chemical landscape of extracellular vesicles, *Nat. Rev. Bioeng.*, 2024, **3**(1), 68–82.
87 C. A. Voigt, Synthetic biology 2020–2030: six commercially-available products that are changing our world, *Nat. Commun.*, 2020, **11**(1), 6379.
88 K. L. Garner, Principles of synthetic biology, *Essays Biochem.*, 2021, **65**(5), 791–811.
89 M. C. Ciferri, Impact of the production method on the properties of erythrocyte-derived extracellular particles: a quantitative and qualitative evaluation, *Nanotheranostics*, 2025, **9**(3), 299–314.